Chapter 2
Empirical Morphological Model to Evaluate Urban Wind Permeability in High-Density Cities

2.1 Introduction

2.1.1 Background

Hong Kong has one of the highest densities among megacities in the world. Seven and a half million inhabitants live on a group of islands that total 1000 km^2. Hong Kong has a hilly topography; hence, only 25% of the land is built-up areas (Ng 2009). Land prices in Hong Kong have been increasing over the years. For example, in the Central Business District, rent prices have increased 33% between 2005 and 2007 (Hong Kong Rating and Valuation Department (HKRVD) 2009). Owing to the limited land area and the increasing land prices, property developers are building taller and bulkier buildings with higher building plot ratios that occupy the entire site area in order to economically cope with the high land costs, as shown in Fig. 2.1. In addition, the Government of Hong Kong has planned the need to deal with an increasing population, which is projected to increase to 10 million in the next 30 years. Seeking ways to optimize the urban morphology of the city is a difficult but important task for urban planners.

Tall and bulky high-rise building blocks with very limited open spaces in between, uniform building heights, and large podium structures have collectively led to lower permeability for urban air ventilation at the pedestrian level (Ng 2009). The mean wind speeds recorded by the urban observatory stations in urban areas over the past decade have decreased by over 40% (Hong Kong Planning Department (HKPD)

Originally published in Edward Ng, Chao Yuan, Liang Chen, Chao Ren and Jimmy C. H. Fung 2011. Improving the wind environment in high-density cities by understanding urban morphology and surface roughness: a study in Hong Kong. Landscape and Urban Planning 101 (1), pp. 59–74, © Elsevier, https://doi.org/10.1016/j.landurbplan.2011.01.004.

C. Yuan, *Urban Wind Environment*, SpringerBriefs in Architectural Design and Technology, https://doi.org/10.1007/978-981-10-5451-8_2

Fig. 2.1 An urban skyline of Hong Kong

2005). Stagnant air in urban areas has caused, among other issues, outdoor urban thermal comfort problems during the hot and humid summer months in Hong Kong. Stagnant air has also worsened urban air pollution by restricting dispersion in street canyon with high building-height-to-street-width ratios. The Hong Kong Environmental Protection Department (HK EPD) has reported the frequent occurrence of high concentrations of pollutants, such as NO_2 and respirable particles (RSP) in urban areas such as Mong Kok and Causeway Bay (Yim et al. 2009). These areas also have some of the highest urban population densities in Hong Kong.

The 2003 outbreak of the Severe Acute Respiratory Syndrome (SARS) epidemic in Hong Kong had brought attention to how environmental factors (i.e., air ventilation and dispersion in buildings) played an important role in the transmission of SARS and other viruses. Since the outbreak, the planning community in Hong Kong started to pay more attention to the urban design process in order to optimize the benefits of the local wind environment for urban air ventilation. As a result, the Hong Kong Government had commissioned a number of studies on this regard; the most important project among the government-commissioned studies is entitled "Feasibility Study for Establishment of Air Ventilation Assessment System" (AVA), which began in 2003 (Ng 2009). The primary purpose of this comprehensive chapter is to establish the protocol that assesses the effects of major planning and development projects on urban ventilation in Hong Kong (Ng 2007).

The importance of wind environment on the heat, mass, and momentum exchange between urban canopy layer and boundary layer has been studied by urban climate researchers (Arnfield 2003). Two modeling methods have been frequently applied to study wind environment of the city: wind tunnel tests and computational fluid dynamics (CFD) techniques. The United States Environmental Protection Agency (US EPA) conducted numerous urban-scale wind tunnel tests to understand the dispersion of particulate matters smaller than 10 μm in aerodynamic diameter (PM_{10}) (Ranade et al. 1990). Williams and Wardlaw (1992) conducted a large-scale wind tunnel study to describe the pedestrian-level wind environment in the city of Ottawa, Canada, and identified areas of concern for planners. Plate (1999) developed the boundary-layer

wind tunnel studies to analyze urban atmospheric conditions, including wind forces on buildings, pedestrian comfort, and diffusion processes from point-sources of the city. Kastner-Klein et al. (2001) analyzed the interaction between wind turbulence and the effects induced by vehicles moving inside the urban canopy. Wind velocity and turbulence scales throughout the street canyons of the city were analyzed using smoke visualization (Perry et al. 2004). In 2004, the US EPA's Office of Research and Development (EPA-ORD) conducted a city-scale wind tunnel study to analyze the airflow and pollutant dispersion in the Manhattan area (Perry et al. 2004). Kubota et al. (2008) conducted wind tunnel tests and revealed the relationship between plan area fraction (λ_p) and the mean wind velocity ratio at the pedestrian level in residential neighborhoods of major Japan cities. In Hong Kong, the Wind/Wave Tunnel Facility has conducted numerous tests at the city, district, and urban scale to understand the wind availability and flow characteristics of Hong Kong (HKPD 2008).

Apart from wind tunnels, CFD model simulation can be applied at the initial urban planning stage in providing a "qualitative impression" of the wind environment. Mochida et al. (1997) conducted a CFD study to analyze the mesoscale climate in the Greater Tokyo area. Murakami et al. (1999) used CFD simulations to analyze the wind environment at the urban scale. Kondo et al. (2006) used CFD simulations to analyze the diffusion of NO_x at the most polluted roadside areas around the Ikegami-Shinmachi crossroads in Japan. Letzel et al. (2008) conducted studies of urban turbulence characteristics using the urban version of the parallelized large eddy simulation (LES) model (PALM), which is superior to the conventional Reynolds-averaged models (RANS). Using the Earth Simulator, Ashie et al. (2009) conducted the largest urban CFD simulation of Tokyo to understand the effects of building blocks on the thermal environment of Tokyo. Ashie et al. noted that the air temperatures around Ginza and JR Shimbashi are much higher than in the surrounding areas of Hama Park and Sumida River. Ashie et al. argued that the high air temperature can be attributed to the bulky buildings at Ginza and JR Shimbashi that obstruct the incoming sea breezes (Ashie et al. 2009). Yim et al. (2009) used CFD simulation to investigate the air pollution dispersion in a typical Hong Kong urban morphology. In general, using CFD for urban-scale investigation has been gaining momentum in the scientific circle. Two important documents that provide guidelines for CFD usage have been published: Architectural Institute of Japan (AIJ) Guidebook (AIJ 2007; Tominaga et al. 2008) and COST action C14 (Frank 2006).

2.1.2 Objectives and Needs of This Study

While the application of wind tunnels and CFD model simulations to analyze the interaction between the urban area and the atmosphere has made important contribution to the understanding of urban air ventilation of the city, such applications are costly, and may not be able to keep up with the fast design process in the initial stages of the design and planning decision-making process. Instead, the outlined and district-based information based on urban morphological data parametrically understood may be more useful for planners.

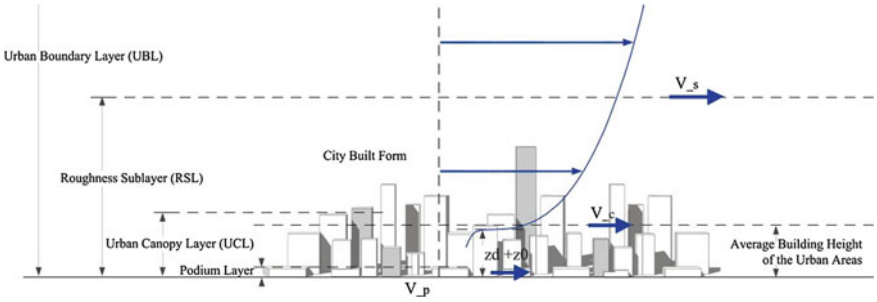

Fig. 2.2 Wind speed profile, podium layer, urban canopy layer, and roughness sublayer. V_{p}: wind speed at the pedestrian level (2 m above the ground); V_{c}: wind speed at the top of urban canopy layer; V_{s}: wind speed at the top of roughness sublayer. The wind speed profile was drawn in accordance with the power law expression: $V\_{z,i}/V\_{500,i} = (Z/500)^{\alpha}$, ($\alpha = 0.35$)

This chapter employs the understandings of urban surface roughness to establish the relationship between heterogeneous urban morphologies and urban air ventilation environment. A new method with cross-section areas, which takes into account the site-specific wind information measured at 60 m height using the MM5/CALMET model simulation, was used to calculate the frontal area density (λ_f). Using the site-specific wind information, the new calculation method of λ_f focuses on the effects of the built environment to the wind field, which provides a spatially averaged understanding of wind permeability at the urban scale.

In addition, the new calculation method of λ_f considers the unique urban morphology of the podiums and towers in Hong Kong (i.e., many tall and slender buildings stand on large podiums), which shows that taking the urban morphology of podiums into consideration is important. Therefore, the podium layer is defined within the urban canopy layer as shown in Fig. 2.2. The spatial characteristics of the large podiums provide much larger drag force on airflow nearer to the ground than the upper layers, and thus can greatly affect the wind environment at the pedestrian level.

This study first correlates the pedestrian-level wind environment with λ_f calculated at the podium layer, and then establishes an understanding of surface roughness and urban morphology based on ground coverage ratio (GCR), a term familiar to urban planners, with λ_f to simplify the practical application of the understanding for professional use.

2.2 Literature Review

2.2.1 Roughness Characteristics

The roughness properties of urban areas affect surface drag, scales and intensity of turbulence, wind speed, and the wind profile in urban areas (Landsberg 1981). The

total drag on a roughness surface includes both a pressure drag (τ_{tp}) on the roughness elements and a skin drag (τ_{ts}) on the underlying surface (Shao and Yang 2005). In this study, only the pressure drag is considered, since skin drag is relatively small and is not a factor that can be controlled at the urban scale. Oke (1987) provided the logarithmic wind profile in a thermally neutral atmosphere, which is a semiempirical relationship that acts as a function of two aerodynamic characteristics: roughness length (z_0) and the zero-plane displacement height (z_d). The reliable evaluation of such aerodynamic characteristics of urban areas is significant in depicting and predicting urban wind behaviors (Grimmond and Oke 1999).

Currently, three methods can be used to estimate the surface roughness: Davenport roughness classification (Davenport et al. 2000), morphologic, and micrometeorological methods (Grimmond and Oke 1999). The Davenport Classification is a surface-type classification based on the assorted surface roughness values, using high-quality observations (Davenport et al. 2000), which covers a wide range of surface types. This method is not too helpful to describe urban permeability in high-density cities, because most of the urban areas could only be described in Class 8 "Skimming: City centre ($z_0 \geq 2$)". Compared with the micrometeorological method, the morphometric method estimates the aerodynamic characteristics, such as z_0 and z_d, using empirical equations (Lettau 1969; MacDonald et al. 1998; Raupach 1992; Bottema 1996; Kutzbach 1961). Grimmond and Oke (1999) validated the empirical models by Kutzbach, Lettau, Raupach, Bottema, and Macdonald. While reasonable relationships between z_0 and frontal area index ($\lambda_{f(\theta)}$) for low- and medium density forms have been found, there is a tendency of overestimation of z_0 for higher density cases (Bottema 1996).

Grimmond and Oke (1999) calculated $\lambda_{f(\theta)}$ in the context of the urban morphology of North America cities. Ratti et al. (2002) calculated $\lambda_{f(\theta)}$ of 36 wind directions in London, Toulouse, Berlin, and Salt Lake City. By incorporating a spatially continuous database on aerodynamic and morphometric characteristics, such as $\lambda_{f(\theta)}$, z_0, and z_d, morphometric estimation methods can be helpful to urban planners and researchers in depicting the distribution of the roughness of the city. Using Bottema's model equation, Gál and Unger (2009) mapped z_0 and z_d to detect the ventilation paths in Szeged. Wong et al. (2010) mapped $\lambda_{f(\theta)}$ to detect the air paths in the Kowloon Peninsula of Hong Kong.

2.2.2 *Calculation of Frontal Area Index and Frontal Area Density*

The frontal area index $\lambda_{f(\theta)}$ is a function of wind direction of θ, which is an important parameter of the wind environment. The $\lambda_{f(\theta)}$ in a particular wind direction of θ is defined (Raupach 1992) as

$$\lambda_{f(\theta)} = \frac{A_F}{A_T} = L_y \cdot Z_H \cdot \rho_{el}, \tag{2.1}$$

where A_F represents the front areas of buildings that face the wind direction of θ, A_T represents the total lot area, L_y represents the mean breadth of the roughness elements that face the wind direction of θ, Z_H represents the mean building height, and ρ_{el} represents the density (number) of buildings per unit area. $\lambda_{f(\theta)}$ has been used widely by researchers in plant canopy and urban canopy communities to help quantify drag force.

Frontal area density, $\lambda_{f(z,\theta)}$, represents the density of $\lambda_{f(\theta)}$ at a height increment of "z" (Burian et al. 2002):

$$\lambda_{f(z,\theta)} = \frac{A\,(\theta)_{proj(\Delta z)}}{A_T}, \tag{2.2}$$

where $A(\theta)_{proj(\Delta z)}$ represents the area of building surfaces that approaches a wind direction of θ for a specified height increment "Δz" and A_T represents the total lot area of the study area.

Compared with $\lambda_{f(\theta)}$, which is an average value that describes the urban morphology of the entire urban canopy, $\lambda_{f(z,\theta)}$ represents a density that describes the urban morphology in the interested height band. Burian et al. (2002) conducted frontal area density calculations in a height increment of 1 m in Phoenix City, and found that $\lambda_{f(z,\theta)}$ is a function of land uses because the buildings in different land uses have different building morphologies.

2.3 Development of New Layer-Based $\lambda_{f(z)}$

Due to the morphological difference between the podium layer and building layer in Hong Kong, as shown in Fig. 2.2, the respective $\lambda_{f(z,\theta)}$ of the layer is expected to be better than $\lambda_{f(\theta)}$ in capturing and describing the complicated urban morphology in Hong Kong. Using a high-resolution (1 × 1 m) three-dimensional building database with building height information and digital elevation model (DEM), a self-developed program embedded as a VBA script in the ArcGIS system was applied to calculate the frontal area density ($\lambda_{f(z)}$) at different height bands. $\lambda_{f(z)}$ accounts for the annual wind probability from 16 main directions:

$$\lambda_{f(z)} = \sum_{\theta=1}^{16} \lambda_{f(z,\theta)} \cdot P_\theta, \tag{2.3}$$

where $\lambda_{f(z,\theta)}$ represents the frontal area density at a particular wind direction (θ), and can be calculated with Eq. 2.2. P_θ represents annual wind probability at a particular direction (θ).

2.3.1 Height of the Podium and Urban Canopy Layer

To identify the height of the podium and urban canopy layer in high-density urban areas of Hong Kong, a statistical study was conducted based on three-dimensional building database provided by the Hong Kong Government. Twenty-five urban areas have been sampled as shown in Fig. 2.3. Mean and upper quartiles of the building and podium height at metropolitan and new town areas were calculated. According to the height distribution shown in Fig. 2.4, the urban canopy layer and podium layer at the metropolitan areas were identified as 60 and 15 m, respectively. Figure 2.5 shows the calculated $\lambda_{f(0–15\ m)}$, $\lambda_{f(15–60\ m),}$ and $\lambda_{f(0–60\ m)}$, corresponding to the height increments of 0–15 m (podium layer), 15–60 m (building layer), and 0–60 m (urban canopy layer), respectively.

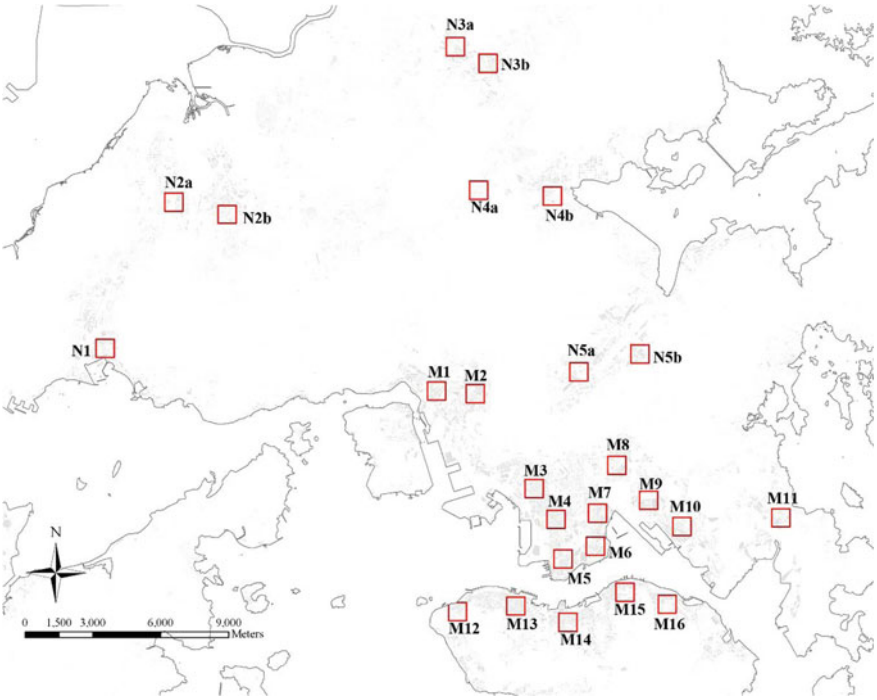

Fig. 2.3 Twenty-five 900 × 900 m test sites (M: Metropolitan areas; N: New town areas)

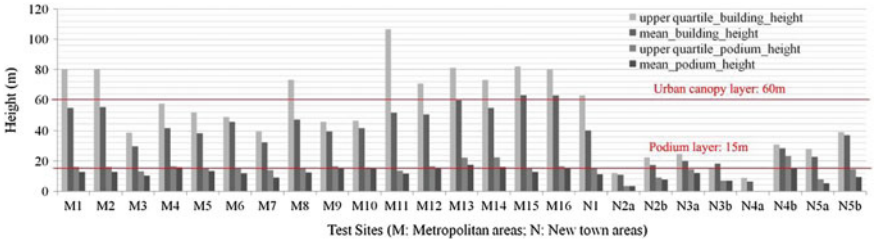

Fig. 2.4 Heights of the urban canopy layer and the podium layer. Based on the understanding, the heights of the urban canopy layer and the podium layer are set in 60 and 15 m for this chapter, respectively

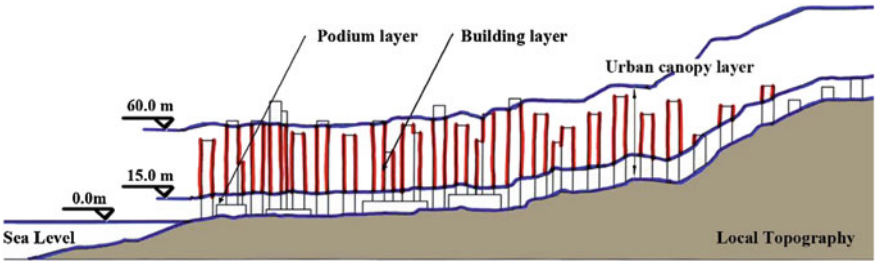

Fig. 2.5 Illustration of the building layer, podium layer and urban canopy layer

2.3.2 Wind Availability in Hong Kong (MM5/CALMET System)

In Hong Kong, the local topography and land–sea contrast impose significant influence on the wind direction in the immediate vicinity of the urban canopy layer, as shown in Fig. 2.5. Therefore, to focus on the impact of building drag force on airflow, site-specific wind roses for annual non-typhoon winds at 60 m height in 16 directions were used to calculate the corresponding local values of $\lambda_{f(z)}$. Due to the complex topography of Hong Kong, the territory is divided into subareas, with various area-specific wind roses (Fig. 2.6). The data on site-specific wind roses were obtained from the fifth-generation NCAR/PSU mesoscale model (MM5) that incorporates the California Meteorological (CALMET) system (Yim et al. 2007). MM5 is a limited-area, non-hydrostatic, and terrain-following mesoscale meteorological model. MM5 is designed to simulate mesoscale and regional-scale atmospheric circulation (Dudhia 1993; Yim et al. 2007). CALMET is a diagnostic three-dimensional meteorological model that can interface with MM5 (Scire et al. 2000).

The terrain in Hong Kong is complex; hence, the resolution used in MM5 simulations (typically down to 1 km) cannot accurately capture the influence of topology characteristics on wind environment. Therefore, CALMET, a prognostic meteorological model capable of higher resolutions (down to 100 m), was used. Combining the data obtained from MM5 and the data obtained from an upper air sounding station,

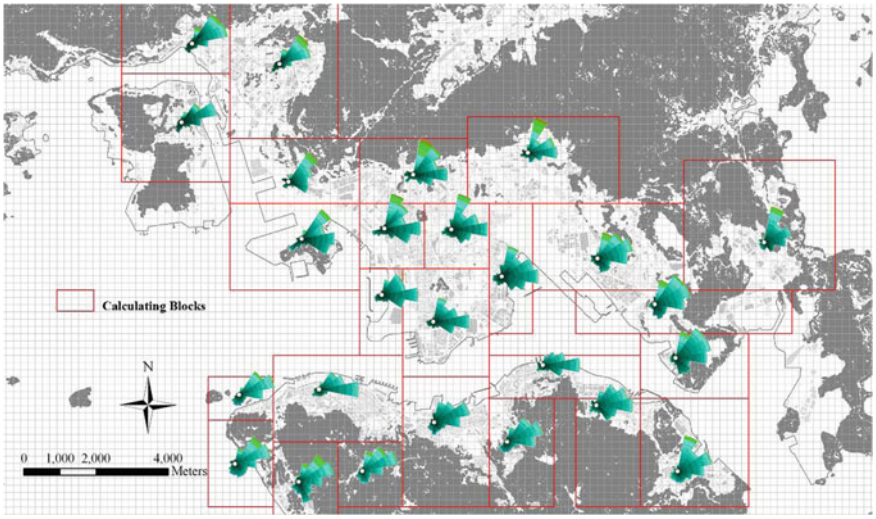

Fig. 2.6 Calculating blocks and representative wind roses at the height of 60 m in 16 directions for annual non-typhoon winds (01/01/2004–12/30/2004). *Data source* Institute for the Environment (IENV) (2010)

maintained by the Hong Kong Observatory, in 2004, the CALMET model adjusts the estimated meteorological fields for the kinematic effects of terrain, slope flows, and terrain blocking effects to reflect the impact of a fine-scale terrain on resultant wind fields at 100 m resolutions (Yim et al. 2007). In the CALMET model simulation, the vertical coordinates were set with 10 levels: 10, 30, 60, 120, 230, 450, 800, 1250, 1750, and 2600 m (Yim et al. 2007).

2.3.3 *Calculation of $\lambda_{f(z)}$ in Grids with Uniform Size*

In this chapter, $\lambda_{f(z)}$ was calculated in uniform grids. Each grid represents a local roughness value. The calculating boundary (grid boundary) was so small that large commercial podiums and public transport stations can be larger than the grid cell and cross the grid boundaries, as shown in Fig. 2.7. Values of $\lambda_{f(z)}$ for the cells at the middle of such large buildings may be underestimated. Therefore, to estimate the local roughness of every grid when buildings cross grid cells, a new method of which the cross-section areas (red areas) were included in the frontal areas of the corresponding grid cell was proposed. Compared with the map in polygon units (Gál and Unger 2009), this new calculation with uniform grid allows an exploration of mapping with a better explanatory power.

Compared with the conventional calculation of $\lambda_{f(z)}$, the nonexisting cross-section walls in the new calculation method could result in unrealistic surface roughness.

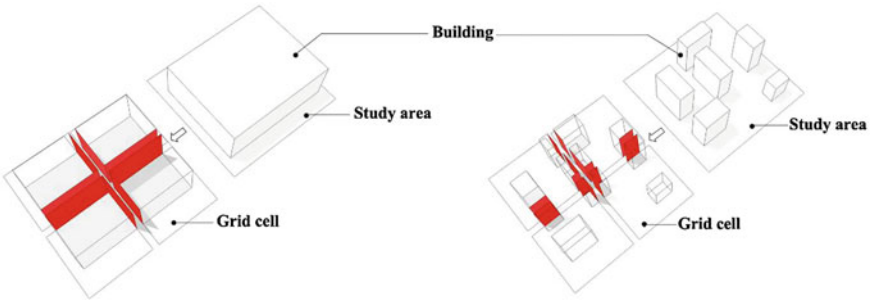

Fig. 2.7 Cross sections (red area) in two examples. When the study area is uniformly divided into four grid cells, the cross sections are generated

However, such cross sections may be needed to avoid underestimation of the surface roughness at the high-density urban areas covered by large and closely packed buildings. Thus, the correlations between the $VR\_{w,j}$ and between the new method of $\lambda_{f(z)}$ with cross section and the traditional method of $\lambda_{f(z)}$ without cross section were compared.

Wind velocity ratios were obtained from wind tunnel tests for Hong Kong (HKPD 2008). The values of $VR\_{w,j}$ of 10 study areas in wind tunnel tests were used as shown in Fig. 2.8. In the wind tunnel tests, test points were uniformly distributed in each study area. $VR\_{w,j}$ for each test point has been described by (HKPD 2008):

$$VR\_{w,j} = \sum_{i=1}^{16} P_i \cdot VR\_{500,i,j}, \tag{2.4}$$

where P_i represents the annual probability of winds approaching the study area from the wind direction (i), and $VR\_{500,i,j}$ represents the directional wind velocity ratio of the jth test point, the mean wind speed at 2 m above the ground with respect to the reference at 500 m (HKPD 2008). $VR\_{500,i,j}$ is defined as (HKPD 2008):

$$VR\_{500,i,j} = \frac{V\_{p,i,j}}{V\_{500,i}} \tag{2.5}$$

where $V\_{p,i,j}$ represents the mean wind speed of the jth test point at the pedestrian level (2 m above the ground) for wind direction (i), and $V\_{500,i}$ represents the mean wind speed of the jth test point at 500 m for wind direction (i).

As emphasized in Fig. 2.9, if study areas in wind tunnel experiment were crossed by grids in the map, the average of $\lambda_{f(z)}$ for the study areas is calculated by

$$\lambda_{f(z)} = \frac{\sum_{i=1}^{4} \lambda_{f\,i\,(z)} \cdot S_i}{S_t}, \tag{2.6}$$

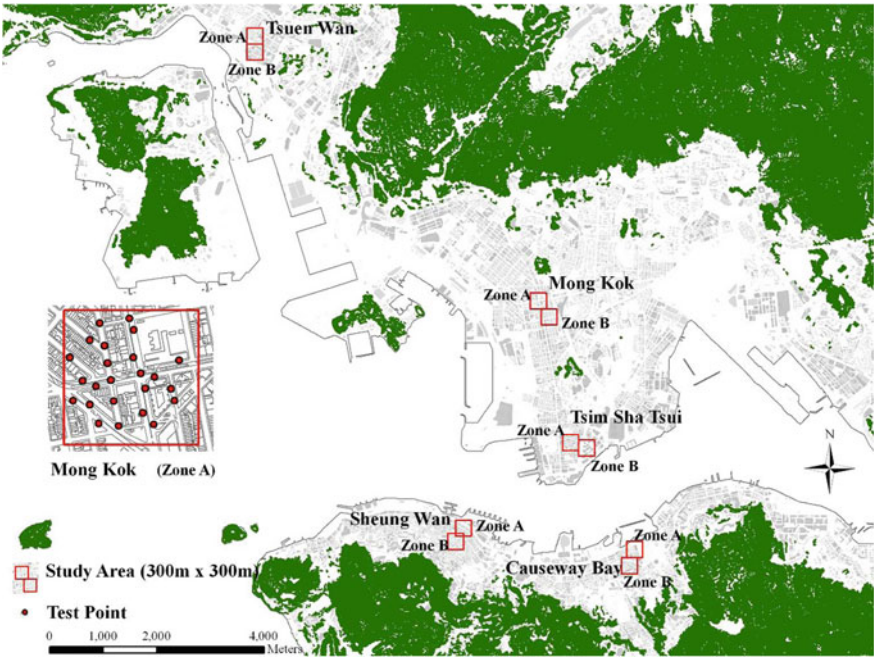

Fig. 2.8 Study areas in the wind tunnel experiment

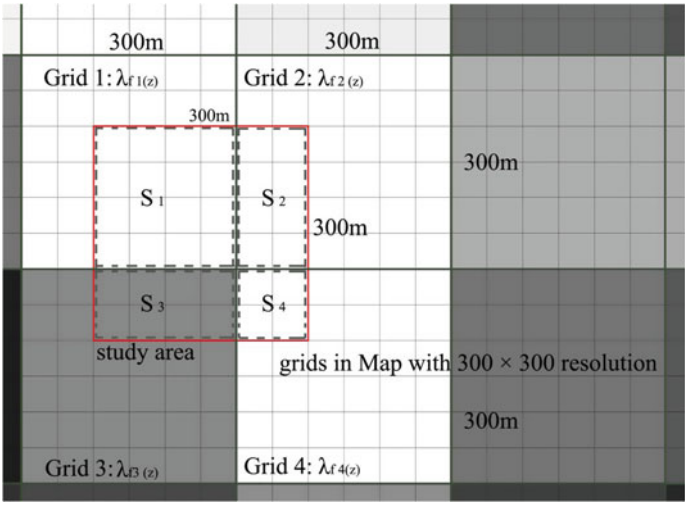

Fig. 2.9 Calculation of the average of $\lambda_{f(z)}$ in the study area (suppose the resolution is 300 × 300 m)

where $\lambda_{f\,i(z)}$ represents the frontal area density in the ith grid, S_i represents the area of the ith grid in the study area, and S_t represents the area of the study.

Table 2.1 Correlation between $VR_{\_w,j}$ and $\lambda_{f(0–15\ m)}$ in different resolutions and calculation methods

	R^2 (with cross sections)	R^2 (no cross sections)
Resolution: 300 × 300 m	0.96	0.96
Resolution: 200 × 200 m	0.87	0.88
Resolution: 100 × 100 m	0.71	0.70
Resolution: 50 × 50 m	0.63	0.66

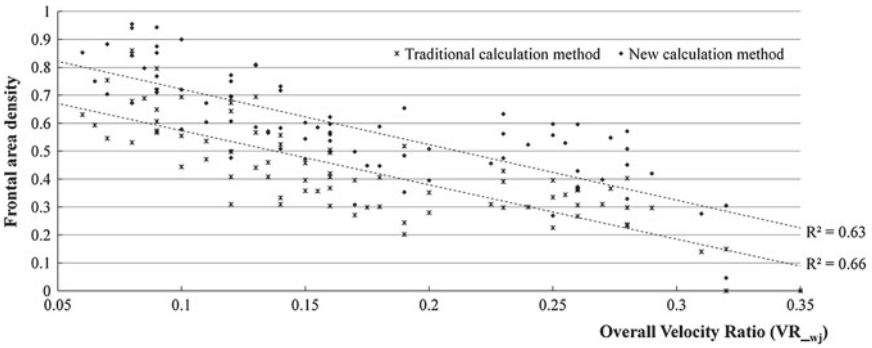

Fig. 2.10 Relationships between $VR_{\_w,j}$ and $\lambda_{f(0–15\ m)}$ calculated by different methods in 50 × 50 m resolutions. The number of the point pairs is 80, and the significance level is 5%

The $\lambda_{f(z)}$ in the podium layer ($\lambda_{f(0–15\ m)}$) that corresponds to the four grid sizes (resolutions), namely 50, 100, 200, and 300 m, were calculated. The R^2 values in Table 2.1 illustrate that the new calculation method can be as accurately predict the wind velocity ratio as the traditional method without cross section. As expected, in accordance with values of the $\lambda_{f(0–15\ m)}$ including the unreal flow-confronting areas were larger than the ones calculated by the traditional method, and their correlations with $VR_{\_w,j}$ were similar (Fig. 2.10).

On the other hand, the $\lambda_{f(0–15\ m)}$ values in the Kowloon Peninsula calculated by the two methods were compared. In high-density urban areas with large and closely packed buildings, the $\lambda_{f(0–15\ m)}$ values calculated by the traditional method without cross section were less than 0.1; some of them were even close to 0. This is a serious underestimation to the surface roughness. Highlighted in Fig. 2.11, the new method with cross section in this chapter efficiently alleviates these underestimations by including the cross sections.

Based on the regression analysis result, following understandings can be stated: the new calculation method with cross sections can correctly predict the wind velocity ratio. Furthermore, compared with the traditional method of calculating frontal area density, the new method can alleviate the underestimation of mapping urban surface roughness in high-density cities with large and closely packed buildings.

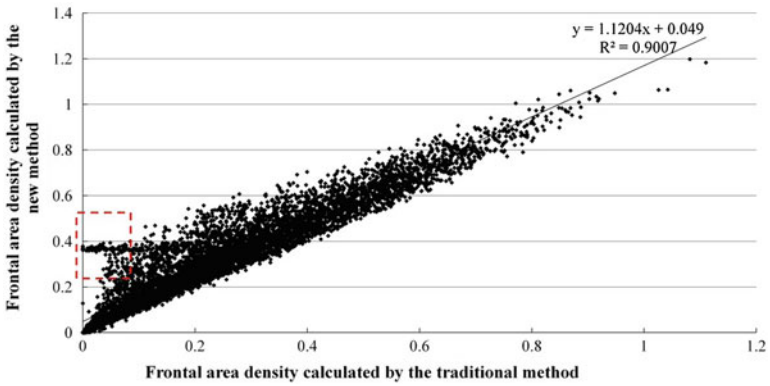

Fig. 2.11 Cross-comparison between $\lambda_{f(0–15\ m)}$ calculated by different methods in 50 × 50 m resolutions (Test area: Kowloon Peninsula). The number of the point pairs is 7519, and the significance level is 5%

2.3.4 Grid Sensitivity (Resolution)

As shown in Table 2.1, the values of R^2 decrease along with the reduction of the grid sizes. Choosing a larger grid size would have a positive effect on depicting the urban wind environment. However, R^2 should not be the only criterion for selecting one grid size over another. For mapping roughness, the explanatory power of the map should not be totally traded off for the sake of the correctness of $\lambda_{f(z)}$. After weighing the considerations, the resolution of 200 × 200 m was adopted in mapping urban permeability in Hong Kong.

2.4 Development of Empirical Model

The skimming flow regime is normally found at the top of compact high-rise building areas (Letzel et al. 2008). Similarly, due to the signature urban morphology of Hong Kong (i.e., high-density and tall buildings), the airflow above the top of the urban canopy layer may not easily enter the deep street canyons to benefit the wind environment at the pedestrian level. Thus, the wind velocity ratio at the pedestrian level mostly depends on the wind permeability of the podium layer. A statistical study was conducted to validate the above assumption by comparing the sensitivities of $VR\_{w,j}$ to changes of $\lambda_{f(z)}$ calculated at different layers. The cross-comparison results are plotted in Fig. 2.12a, b, which indicate that $VR\_{w,j}$ has a higher correlation with $\lambda_{f(z)}$ at the podium layer (0–15 m). This illustrates that pedestrian-level wind speed depends on the urban morphology at the podium layer (0–15 m), rather than the building layer (15–60 m) or the whole canopy layer (0–60 m).

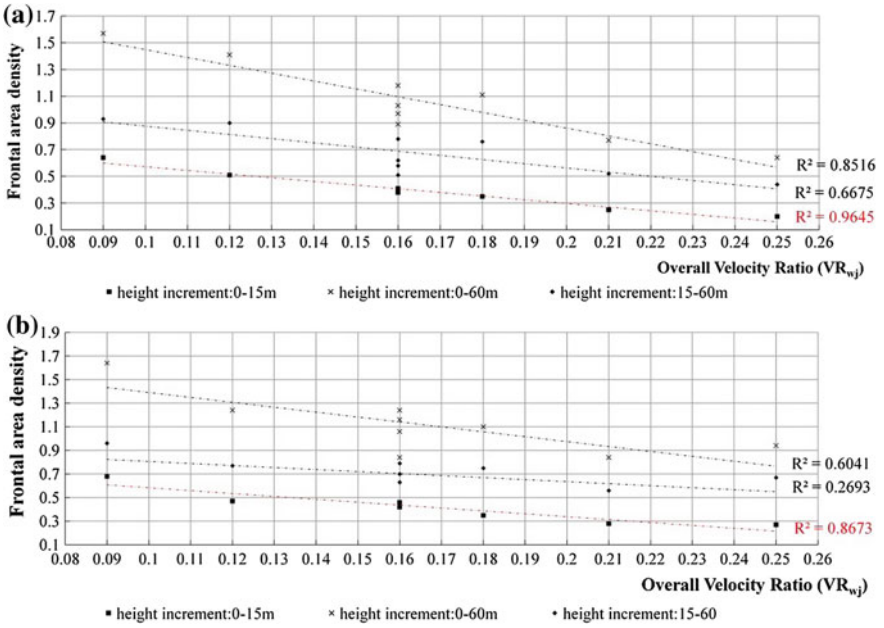

Fig. 2.12 **a** Relationships between overall velocity ratio (VR$_{_w,j}$) and averaged $\lambda_{f(0–15\ m)}$, $\lambda_{f(15–60\ m)}$, and $\lambda_{f(0–60\ m)}$ in 300 × 300 m resolutions. The number of the point pairs is 9, and the significance level is 5%. **b** Relationships between overall velocity ratio (VR$_{_w,j}$) and averaged $\lambda_{f(0–15\ m)}$, $\lambda_{f(15–60\ m)}$, and $\lambda_{f(0–60\ m)}$ in 200 × 200 m resolutions. The number of the point pairs is 9, and the significance level is 5%

2.5 Implementation in Urban Planning

2.5.1 Mapping Urban Wind Permeability Using $\lambda_{f(z)}$

This understanding is important to support the evidence-based urban planning and design in order to improve the pedestrian-level wind environment at high-density urban areas. Compared with front area index, which was used to detect the air paths in Hong Kong (Wong et al. 2010), $\lambda_{f(0–15\ m)}$ has been proven to be a better morphological factor in depicting the wind environment at the pedestrian level. As shown in Fig. 2.13a, the map of the frontal area density (0–15 m) depicts the local wind permeability at the podium layer in the Kowloon Peninsula and Hong Kong Island. The continuous belts of high surface roughness on the northern coastline of the Hong Kong Island and both sides of the Kowloon peninsula, referred to as the wall effect of the Kowloon Peninsula, are evident (Yim et al. 2009), whereas the wind permeability is very low. The maps of the frontal area density (0–60 m and 15–60 m) are also presented, as shown in Fig. 2.13b, c. These two maps are important for describing the wind permeability at the urban canyon layer. The turbulent mixing at the urban

canyon layer is essential to improve urban air ventilation, alleviate air pollution, and dissipate the anthropogenic heat.

2.5.2 Ground Coverage Ratio and Frontal Area Density

Compared with $\lambda_{f(z)}$, ground coverage ratio (GCR) is a two-dimensional parameter commonly used by urban planners. GCR is defined as

$$\mathrm{GCR} = \frac{A_b}{A_T} = \frac{w^2 \cdot n}{A_T}, (n \geq 1), \tag{2.7}$$

where A_T represents the site area, A_b represents the built area, w represents the average building width, and n represents the number of buildings. A statistical study was conducted to convert the frontal area density analysis to a practical design and planning tool; this was accomplished by investigating the relationship between $\lambda_{f(0–15\ m)}$ and GCR.

Local values of $\lambda_{f(0–15\ m)}$ and the GCR of the 1004 test areas (200 × 200 m) in the Kowloon Peninsula and the Hong Kong Island were calculated. Figure 2.14 shows a good linear relationship of both ($R^2 = 0.77$). However, it should be noted the presence of outlier values of local surface roughness of large podiums and industrial buildings.

Equation 2.8 indicates the relationship between GCR and $\lambda_{f(z)}$, which depends on k, the ratio between the averaged building width (w) and podium layer height, i.e. 15 m. If the building width of urban areas is much larger than that of other areas with normal building morphology, the correlation between GCR and $\lambda_{f(0–15\ m)}$ in such areas can be significantly different from other areas. Four examples of such sites, points A–D, are shown in Figs. 2.14 and 2.15.

$$\mathrm{GCR} = \frac{w \cdot \lambda_{f(0-15\,m)}}{15} = k \cdot \lambda_{f(0-15\,m)}, \quad k = \frac{w}{15}. \tag{2.8}$$

Based on the above discussion, following understandings can be stated:

(1) There is a good linear relationship between $\lambda_{f(0–15\ m)}$ and GCR ($R^2 = 0.77$) in most of the test points. For planners, using GCR to predict the wind environment at the pedestrian level is reasonable. Compared with other traditional maps (Gál and Unger 2009; Wong et al. 2010), the proposed GCR map is more applicable to urban designers and planners due to its accessibility to the planners in the planning process.

(2) Local values of some areas may deviate due to the extremely large building widths (large commercial podiums and industrial buildings). In this type of areas, the wind permeability cannot be predicted in GCR. However, the occurrence of this type of extreme examples is very small (approximately 2%).

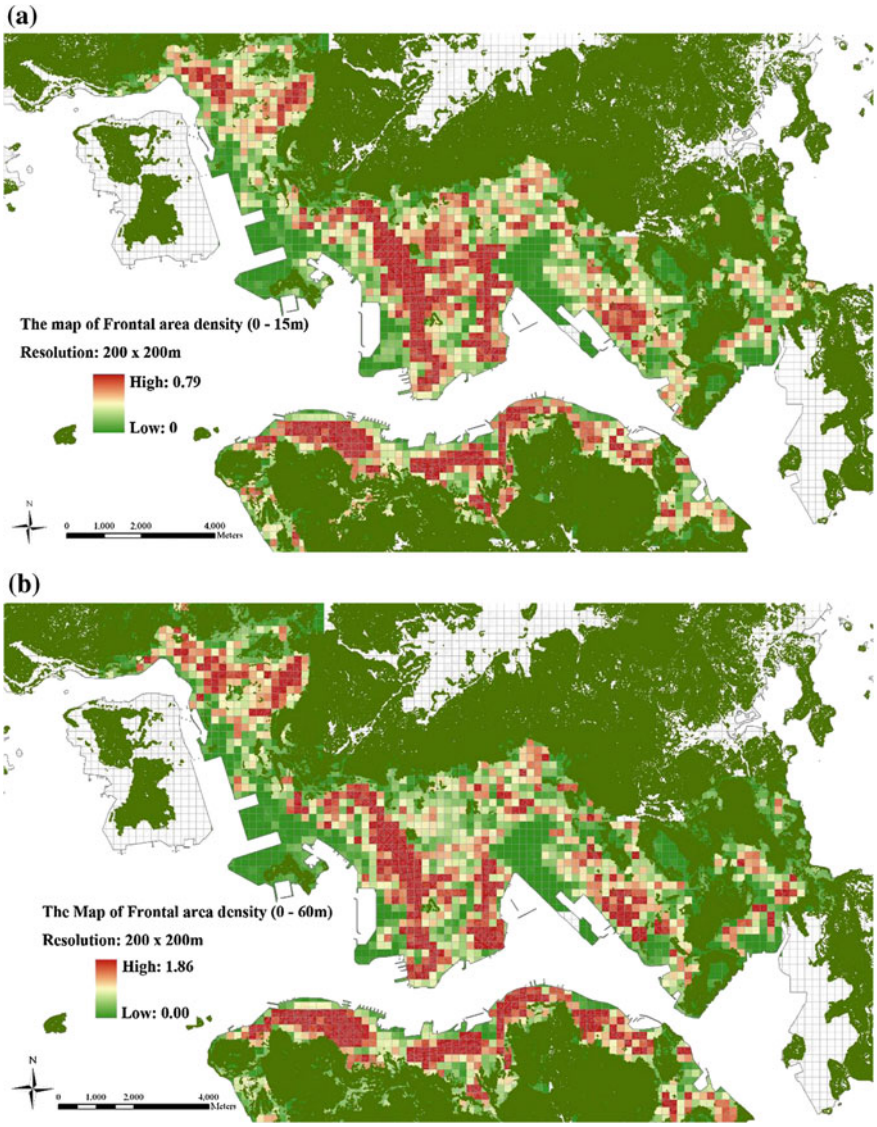

Fig. 2.13 **a** Map of frontal area density in Kowloon and Hong Kong Island (Resolution: 200 × 200 m, height increment (Δz): 0–15 m) (For interpretation of the references to color in the text, the reader is referred to the electronic version of this book). **b** Map of frontal area density in Kowloon and Hong Kong Island (Resolution: 200 × 200 m, height increment (Δz): 0–60 m) (For interpretation of the references to color in the text, the reader is referred to the electronic version of this book). **c** Map of frontal area density in Kowloon and Hong Kong Island (Resolution: 200 × 200 m, height increment (Δz): 15–60 m (For interpretation of the references to color in the text, the reader is referred to the electronic version of this book)

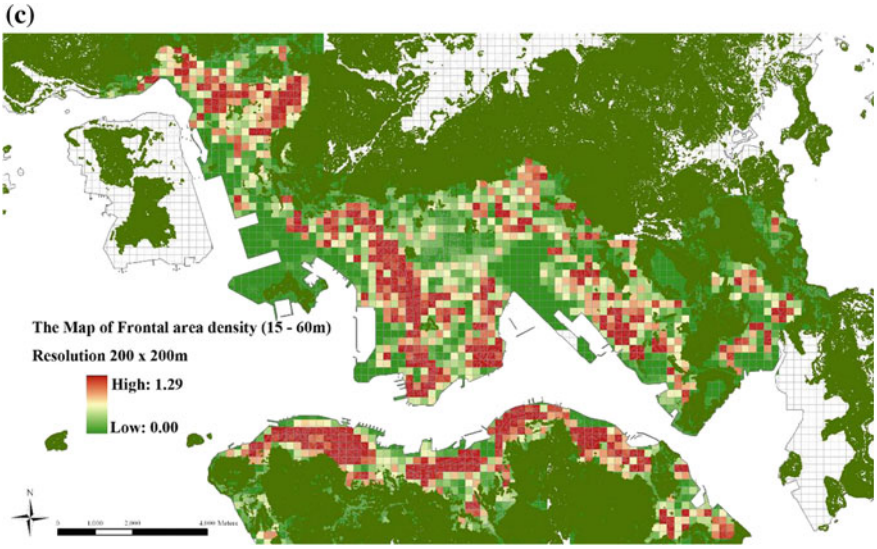

Fig. 2.13 (continued)

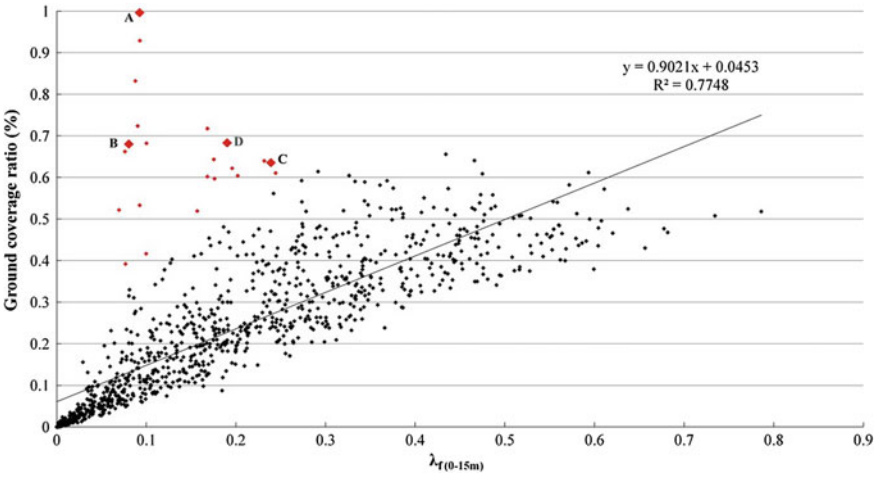

Fig. 2.14 Relationship between $\lambda_{f(0–15\ m)}$ and GCR in Kowloon Peninsula and Hong Kong Island. The outlier values were highlighted in red. The points A, B, C, and D correspond to the four examples in Fig. 2.15. The number of the point pairs is 1032, and the significance level is 5%

2.5.3 Mapping Urban Wind Permeability Using GCR

An urban-level wind environment of Hong Kong was mapped using GCR information in this section. Kubota et al. (2008) and Yoshie et al. (2008) conducted an earlier investigation on the relationship between GCR and the spatial average of wind veloc-

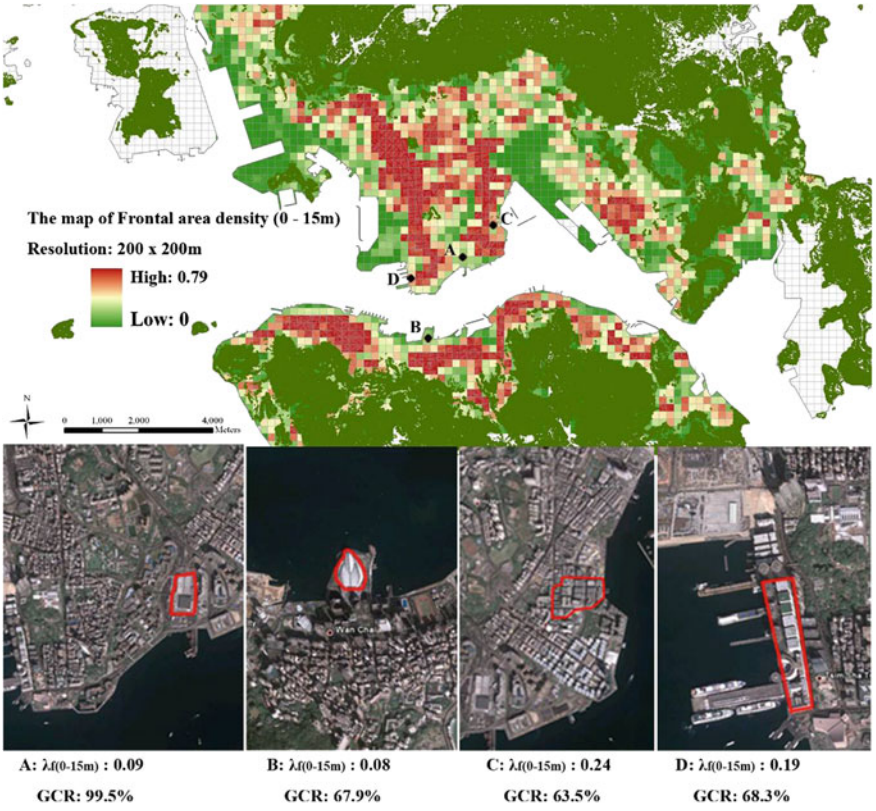

Fig. 2.15 Four typical cases highlighted in Fig. 2.14

ity ratios at a height of 1.5 m obtained by wind tunnel tests, both in Japanese cities and in the Mong Kok area of Hong Kong. This relationship can be used as the basis for the threshold values of the map classification. Coupled with the classification, the effect of different GCRs on the wind permeability can be identified. As shown in Fig. 2.16, three classification values are assigned: "Class 1", "Class 2", and "Class 3", which denote good, reasonable, and poor pedestrian wind performance, respectively.

Based on this classification, the map of wind performance at the podium layer in Hong Kong was generated as shown in Fig. 2.17. Compared with the roughness map without classification, the map in this study is more intuitive; in addition, it allows urban planners to better modify building morphology in order to improve the urban air environment. Such map can be the spatial reference for urban planners.

After incorporating the respective site-specific wind roses, the areas with low wind permeability are depicted in Fig. 2.17. These areas block wind and worsen the wind environment at the pedestrian level of their leeward districts. Potential air paths in the podium layer are also marked out in this map. The potential air paths would play an important role to improve the urban ventilation and environment quality by

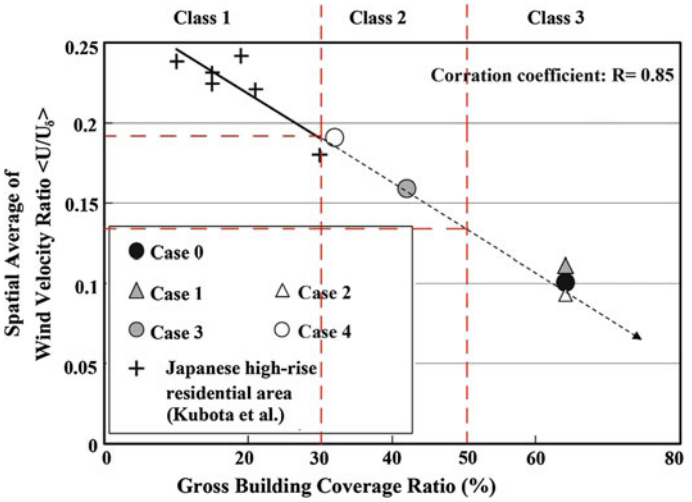

Fig. 2.16 Relationship between ground coverage ratio and spatial average of wind velocity ratios in Mong Kok and cities in Japan (Kubota et al. 2008; Yoshie et al. 2008, edited by authors). The number of the point pairs is 11

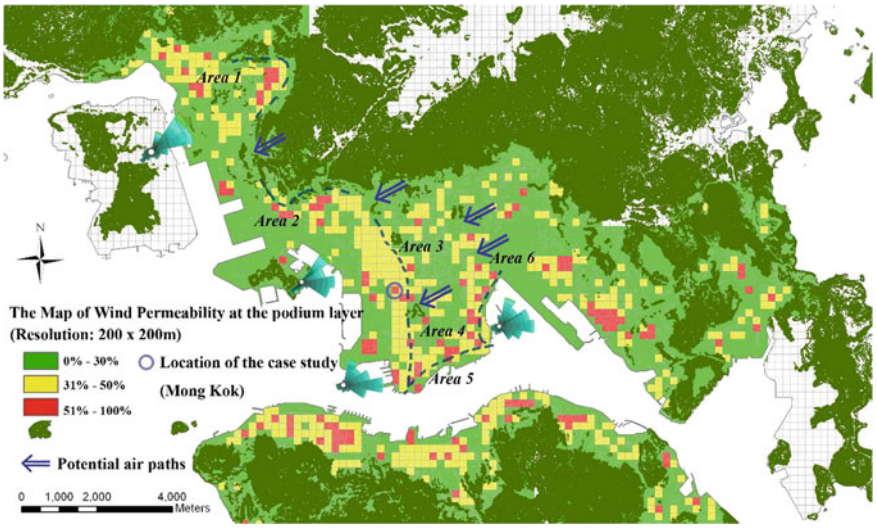

Fig. 2.17 Map of wind permeability at the podium layer. The wind permeability at the podium level is depicted in the map: Class 1: GCR = 0–30%, Class 2: GCR = 31–50%, and Class 3: GCR > 50%. Based on the respective annual prevailing wind direction, the areas with low wind permeability are pointed out. These areas could block the natural ventilation and worsen the leeward districts' wind environment at the pedestrian level. Potential air paths in the podium layer are also marked out in this map (For interpretation of the references to color in the text, the reader is referred to the electronic version of this book)

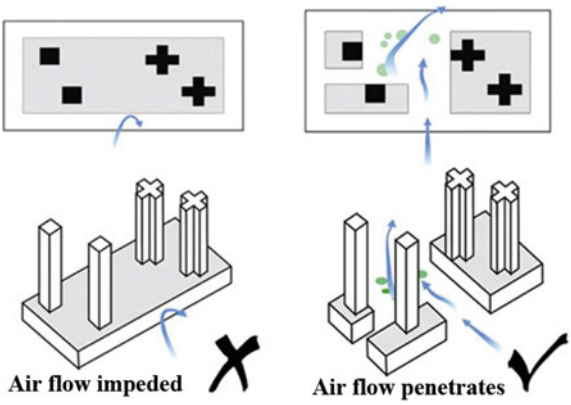

Fig. 2.18 Podium designs as in the HKPSG

bringing fresh airflow into the urban areas for the purpose of dissipating air pollutant and mitigating urban heat island intensity.

2.6 Conclusions

The chapter has highlighted a number of important points that should be considered by city planners. First, one of the most significant factors is urban morphology, especially the podium layer, and its implication to the urban air ventilation environment. According to Chap. 11, Sects. 9–13 of the Hong Kong Planning Standards and Guidelines (HKPSG) (HKPD 2006), a number of urban forms deemed to be conducive to the urban air ventilation environment have been proposed:

> … it is critical to increase the permeability of the urban fabric at the street levels. Compact integrated developments and podium structures with full or large ground coverage on extensive sites typically found in Hong Kong are particularly impeding air movement and should be avoided where practicable. The following measures should be applied at the street level for large development/redevelopment sites particularly in the existing urban areas:
>
> - providing setback parallel to the prevailing wind;
> - designating non-building areas for sub-division of large land parcels;
> - creating voids in facades facing wind direction; and/or
> - reducing site coverage of the podia to allow more open space at grade.

Where appropriate, a terraced podium design should be adopted to direct downward airflow to the pedestrian level as shown in Figs. 2.18 and 2.19.

This chapter shows that the qualitative understanding of the podium structure, as mentioned in the HKPSG, is valid. In Hong Kong, some areas of high podium coverage can be identified. These areas require the most significant design, planning intervention and improvement.

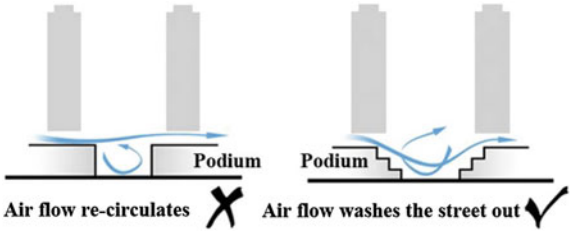

Fig. 2.19 Terraced podium designs as in the HKPSG

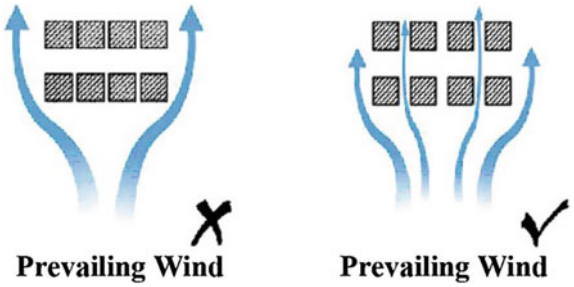

Fig. 2.20 Building dispositions as in the HKPSG

For building block disposition, the chapter has emphasized that city planners need to factor in the prevailing wind understanding to street layout and building disposition design as shown in Fig. 2.20. This understanding is in line with the concerns of the so-called "wall buildings", wherein a line of tall buildings screen the waterfront from the inland areas, thereby blocking the incoming urban air ventilation from the sea.

Based on the GCR information readily available to planners working on their GIS system, the chapter has shown that planners can easily generate an urban wind permeability map, thereby enhancing the possibility to identify problem areas and, more importantly, to emphasize on potential air paths. The map also enables the interconnectivity of open spaces for urban air ventilation, and allows planners to take urban breezeways into account and design in accordance with the recommendations of the HKPSG (HKPD 2006), as shown in Fig. 2.21:

> For better urban air ventilation in a dense, hot-humid city, breezeways along major prevailing wind directions and air paths intersecting the breezeways should be provided in order to allow effective air movements into the urban area to remove heat, gases and particulates and to improve the micro-climate of urban environment.
>
> Breezeways should be created in forms of major open ways, such as principal roads, interlinked open spaces, amenity areas, non-building areas, building setbacks and low-rise building corridors, through the high-density/high-rise urban form. They should be aligned primarily along the prevailing wind direction routes, and as far as possible, to also preserve and funnel other natural airflows including sea and land breezes and valley winds, to the developed area.
>
> The disposition of amenity areas, building setbacks and non-building areas should be linked, and widening of the minor roads connecting to major roads should be planned in such a way to form ventilation corridors/air paths to further enhance wind penetration into inner parts of urbanized areas. For effective air dispersal, breezeways and air paths should be perpendicular or at an angle to each other and extend over a sufficiently long distance for continuity.

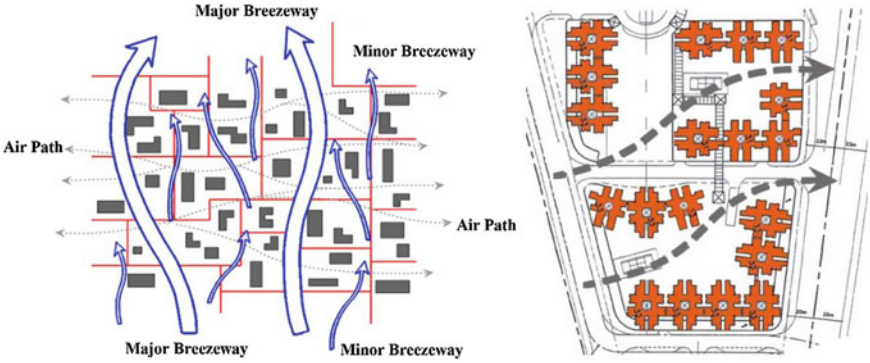

Fig. 2.21 Breezeway and air path design as in the HKPSG

Using the urban wind permeability map of the territory, city planners can initially estimate the possible urban air ventilation environment of the urban areas with the average velocity ratios. Adjusting the pedestrian-level wind speeds and predicting the bioclimatic conditions of the city have become possible.

Overall, the chapter has demonstrated a practical and reliable way for city planners to quickly obtain district-level urban air ventilation information for their board-based design works at the early stages. Conceptually, avoiding wrong decisions that may be difficult to rectify later is, therefore, possible.

References

Architectural Institute of Japan (AIJ) (2007) AIJ guidebook for practical applications of CFD to pedestrian wind environment around buildings (ISBN 978-4-8189-2665-3)

Arnfield AJ (2003) Two decades of urban climate research: a review of turbulence, exchanges of energy and water, and the urban heat island. Int J Climatol 23(1):1–26

Ashie Y, Hirano K, Kono T (2009) Effects of sea breeze on thermal environment as a measure against Tokyo's urban heat island. Paper presented at the seventh international conference on urban climate, Yokohama, Japan

Bottema M (1996) Roughness parameters over regular rough surfaces: Experimental requirements and model validation. J Wind Eng Ind Aerodyn 64(2–3):249–265

Burian SJ, Velugubantla SP, Brown MJ (2002) Morphological analyses using 3D building databases: Phoenix, Arizona. Los Alamos National Laboratory, LA-UR-02-6726

Davenport AG, Grimmond CSB, Oke TR, Wieringa J (2000) Estimating the roughness of cities and sheltered country. Paper presented at the proceedings of the 12th conference on applied climatology, Boston

Dudhia J (1993) A nonhydrostatic version of the penn state-NCAR mesoscale model: validation tests and simulation of an Atlantic cyclone and cold front. Mon Weather Rev 121:1493–1513

Frank J (2006) Recommendations of the COST action C14 on the use of CFD in predicting pedestrian wind environment. J Wind Eng 108:529–532

Gál T, Unger J (2009) Detection of ventilation paths using high-resolution roughness parameter mapping in a large urban area. Build Environ 44(1):198–206

Grimmond CSB, Oke TR (1999) Aerodynamic properties of urban areas derived from analysis of surface form. J Appl Meteorol 38:1262–1292
Hong Kong Planning Department (HKPD) (2005) Feasibility study for establishment of air ventilation assessment system. Final report, The government of the Hong Kong Special Administrative Region
Hong Kong Planning Department (HKPD) (2006) Hong Kong planning standards and guidelines. The government of the Hong Kong Special Administrative Region
Hong Kong Planning Department (HKPD) (2008) Urban climatic map and standards for wind environment—feasibility study. Working paper 2B: wind tunnel benchmarking studies, Batch I. The government of the Hong Kong Special Administrative Region
Hong Kong Rating and Valuation Department (HKRVD) (2009) Private office—1984–2007 Rental and price indices for Grade A Office in core districts. The government of the Hong Kong Special Administrative Region
Institute for the Environment (IENV) (2010) Study of ventilation over Hong Kong. The Hong Kong University of Science and Technology
Kastner-Klein P, Fedorovich E, Rotach MW (2001) A wind tunnel study of organised and turbulent air motions in urban street canyons. J Wind Eng Ind Aerodyn 89(9):849–861
Kondo H, Asahi K, Tomizuka T, Suzuki M (2006) Numerical analysis of diffusion around a suspended expressway by a multi-scale CFD model. Atmos Environ 40(16):2852–2859
Kubota T, Miura M, Tominaga Y, Mochida A (2008) Wind tunnel tests on the relationship between building density and pedestrian-level wind velocity: development of guidelines for realizing acceptable wind environment in residential neighborhoods. Build Environ 43(10):1699–1708
Kutzbach J (1961) Investigations of the modifications of wind profiles by artificially controlled surface roughness. University of Wisconsin—Madison, Madison
Landsberg HE (1981) The urban climate, vol 28. Academic Press, INC. (London) LTD., London
Lettau H (1969) Note on aerodynamic roughness-parameter estimation on the basis of roughness-element description. J Appl Meteorol 8:828–832
Letzel MO, Krane M, Raasch S (2008) High resolution urban large-eddy simulation studies from street canyon to neighbourhood scale. Atmos Environ 42(38):8770–8784
MacDonald RW, Griffiths RF, Hall DJ (1998) An improved method for the estimation of surface roughness of obstacle arrays. Atmos Environ 32(11):1857–1864
Mochida A, Murakami S, Ojima T, Kim S, Ooka R, Sugiyama H (1997) CFD analysis of mesoscale climate in the Greater Tokyo area. J Wind Eng Ind Aerodyn 67–68:459–477
Murakami S, Ooka R, Mochida A, Yoshida S, Kim S (1999) CFD analysis of wind climate from human scale to urban scale. J Wind Eng Ind Aerodyn 81(1–3):57–81
Ng E (2007) Feasibility study for establishment of air ventilation assessment system (AVAS). HKIP J 22(1):39–45
Ng E (2009) Policies and technical guidelines for urban planning of high-density cities—air ventilation assessment (AVA) of Hong Kong. Build Environ 44(7):1478–1488
Oke TR (1987) Boundary layer climates, 2nd edn. Methuen Inc, USA
Perry SG, Heist DK, Thompson RS, Snyder WH, Lawson RE (2004) Wind tunnel simulation of flow and pollutant dispersal around the World Trade Centre site. Environ Manager 31–34
Plate EJ (1999) Methods of investigating urban wind fields—physical models. Atmos Environ 33(24–25):3981–3989
Ranade MB, Woods MC, Chen FL, Purdue LJ, Rehme KA (1990) Wind tunnel evaluation of PM10 samplers. Aerosol Sci Technol 13(1):54–71
Ratti C, Sabatino SD, Britter R, Brown M, Caton F, Burian S (2002) Analysis of 3-D urban databases with respect to pollution dispersion for a number of European and American cities. Water Air Soil Pollut Focus 2:459–469
Raupach MR (1992) Drag and drag partition on rough surfaces. Bound-Layer Meteorol 60:375–395
Scire JS, Robe FR, Fernau ME, Yamartino RJ (2000) A user's guide for the CALMET meteorological model (Version 5). Earth Tech Inc, Concord, MA, USA

Shao Y, Yang Y (2005) A scheme for drag partition over rough surfaces. Atmos Environ 39(38):7351–7361

Tominaga Y, Mochida A, Yoshie R, Kataoka H, Nozu T, Yoshikawa M, Shirasawa T (2008) AIJ guidelines for practical applications of CFD to pedestrian wind environment around buildings. J Wind Eng Ind Aerodyn 96:1749–1761

Williams CD, Wardlaw RL (1992) Determination of the pedestrian wind environment in the city of Ottawa using wind tunnel and field measurements. J Wind Eng Ind Aerodyn 41(1–3):255–266

Wong MS, Nichol JE, To PH, Wang J (2010) A simple method for designation of urban ventilation corridors and its application to urban heat island analysis. Build Environ 45(8):1880–1889

Yim SHL, Fung JCH, Lau AKH, Kot SC (2007) Developing a high-resolution wind map for a complex terrain with a coupled MM5/CALMET system. J Geophys Res 112:D05106

Yim SHL, Fung JCH, Lau AKH, Kot SC (2009) Air ventilation impacts of the "wall effect" resulting from the alignment of high-rise buildings. Atmos Environ 43(32):4982–4994

Yoshie R, Tanaka H, Shirasawa T, Kobayashi T (2008) Experimental study on air ventilation in a built-up area with closely-packed high-rise building. J Environ Eng 627:661–667(in Japanese)